ELSEVIER

Journal of Chromatography A, 925 (2001) 1–17

JOURNAL OF CHROMATOGRAPHY A

www.elsevier.com/locate/chroma

Comparative modeling of breakthrough curves of bovine serum albumin in anion-exchange chromatography

Krzysztof Kaczmarski[a,b,1], Dorota Antos[c], Hong Sajonz[a,b,2], Peter Sajonz[a,b,3], Georges Guiochon[a,b,*]

[a]*Department of Chemistry, The University of Tennessee, Knoxville, TN 37996-1600, USA*
[b]*Division of Chemical and Analytical Sciences, Oak Ridge National Laboratory, Oak Ridge, TN 37831-6120, USA*
[c]*Faculty of Chemistry, Rzeszów University of Technology, W. Pola 2 Street, 35-959 Rzeszów, Poland*

Received 26 February 2001; received in revised form 5 June 2001; accepted 5 June 2001

Abstract

The experimental results of a previous study of the mass transfer kinetics of bovine serum albumin (BSA) in ion-exchange chromatography, under nonlinear conditions, were reevaluated using the general rate model of chromatography. Solutions of this model were obtained numerically. The influences of axial dispersion, the resistance to mass transfer from the bulk mobile phase to the surface of the packing particles, and the intraparticle mass transfer resistances on the profiles of the breakthrough curves of BSA were investigated. The results obtained are compared to those of a previous investigation of the same data, using the simple transport–dispersive model and the lumped pore diffusion model. The results obtained show that the use of an oversimplified model for the analysis of chromatographic data can lead to erroneous interpretations of the experimental data and to misunderstandings of the fundamentals of the processes involved. Finally, a theoretical comparison between the properties and the range of application of the three models is provided.

Keywords: Kinetic studies; General rate model; Lumped pore diffusion model; Transport–dispersive model; Equilibrium–dispersive model; Mathematical modeling; Mass transfer; Breakthrough volumes; Dispersion; Albumin

1. Introduction

Numerous mathematical models are available to account for the band profiles obtained in chromatography and in other adsorption-based separation processes [1–3]. When the mass transfer resistances are small and have a minor influence on the profiles, the equilibrium–dispersive (ED) model is recommended [3]. Otherwise, depending on the nature and the complexity of the problem, the general rate (GR) model, the lumped pore diffusion (POR) model, or the transport–dispersive (TD) model are used (see

*Corresponding author. Department of Chemistry, The University of Tennessee, 552 Buehler Hall, Knoxville, TN 37996-1600, USA. Tel.: +1-865-9740-733; fax: +1-865-9742-667.
E-mail address: guiochon@utk.edu (G. Guiochon).
[1]On leave from the Faculty of Chemistry, Rzeszów University of Technology, W. Pola 2 Street, 35-959 Rzeszów, Poland.
[2]Present address: L'Oréal, Analytical R&D, Clark, NJ, USA.
[3]Present address: Merck Research Laboratories, Rahway, NJ, USA.

0021-9673/01/$ – see front matter
PII: S0021-9673(01)01035-4

e.g., Refs. [4–8]). The GR model is the most general model of chromatography. In this model, axial dispersion and all the mass transfer resistances are taken into consideration, namely (1) the external mass transfer of the solute molecules from the bulk phase to the external surface of the adsorbent particles; (2) the diffusive transport through the pores of these particles; and (3) the adsorption–desorption processes at the actual sites [1–3]. However, the GR model is used only reluctantly because of the relatively large number of parameters needed to characterize the axial dispersion, the external mass transfer, and the effective diffusion through the pores, including the external bed porosity and the adsorbent particle porosity. These coefficients should be known for a predictive use of the model and some of them are difficult to measure accurately. The use of the simpler POR model also requires knowledge of the values of several of these parameters. Therefore, the simple TD model is frequently used when the mass transfer resistances have a moderate influence on the profiles of chromatographic bands. To solve this model, we need to know only the value of the dispersion coefficient, the overall mass transfer coefficient, and the total bed porosity. These coefficients can be derived from a few simple measurements.

The TD model was recently used for a study of mass transfer in anion-exchange chromatography [6–8]. It was shown that, in order correctly to describe experimental breakthrough curves, it had to be assumed that the overall mass transfer coefficient depends on the concentration. This result was not original; it had been previously reported in numerous publications [9–15]. For example, Friedrich et al. [9] reported that the rate of surface diffusion on carbon adsorbents increases rapidly with increasing concentration. Lederer et al. [10] showed that axial dispersion in size-exclusion chromatography increases with increasing concentration. It was shown that the diffusion coefficient [11], the axial dispersion [12], and the mass transfer rate coefficients [13] of proteins in chromatography increase with increasing concentration. So does also the effective diffusivity of different solutes in bulk solutions [14]. All these investigations were based on the use of the TD model to account for the experimental data. Finally, Seidel-Morgenstern et al. [15] showed that the apparent axial dispersion of the two enantiomers of Tröger's base on microcrystalline cellulose triacetate decreases significantly with increasing concentration. This last study was based on the use of the equilibrium–dispersive model, lumping the mass transfer kinetics with axial dispersion.

Nevertheless, this concentration dependence of the mass transfer coefficient is somewhat unexpected. It is important to determine whether it is an actual physical effect or whether it arises from a model error, the TD model being too simple to account for the complex phenomena involved in the phase equilibration when the mass transfer kinetics is too slow compared to the rate of convective transfer of the band. In all the cases in which a concentration dependence of the mass transfer rate coefficient was found, the experimental data were not fitted to the more complex POR or GR models. A comparison between band profiles calculated with the GR, the POR and the ED models was presented earlier [16]. This work showed that, in high concentration chromatography (i.e., under such conditions that the economic efficiency of preparative separations is high and close to its maximum), the GR model can be replaced by the POR model when:

$$\mathrm{Pe} > 100 \quad \frac{\mathrm{St}}{\mathrm{Bi}} > 5$$

where Pe is the Peclet number [$\mathrm{Pe} = uL/(D_L \epsilon_e)$], St the Stanton number ($\mathrm{St} = k_{ext} a_p L \epsilon_e / u$), and Bi the Biot number ($\mathrm{Bi} = k_{ext} d_p / 2D_{eff}$), with u, mobile phase velocity, d_p average particle diameter, L, column length, k_{ext} external mass transfer coefficient, and D_{eff} effective diffusion coefficient. It was also shown [16] that the ED model could be preferred to the POR model when:

$$\mathrm{Pe} > 100 \quad \frac{\mathrm{St}}{1 + \mathrm{Bi}/5} > 2000$$

$$\mathrm{Pe} > 500 \quad \frac{\mathrm{St}}{1 + \mathrm{Bi}/5} > 4000$$

If these conditions are not fulfilled, important or even major differences are observed between the numerical solutions of these different models, the results closest to experimental data being those obtained with the GR model. Although this earlier work did not involve the TD model, its conclusions suggest a plausible explanation for the concentration

dependence of the rate coefficient, a model error arising from the simplifying assumption made in the ED and TD models that the concentration of the feed components is always homogeneous across the particles.

The goals of this work are to reevaluate previous experimental data on the mass transfer kinetics of bovine serum albumin (BSA) in anion-exchange chromatography [6,17], using the GR and the POR models, and to determine the conditions under which the TD model can be used instead of the more complex POR or GR ones and still give similar numerical solutions.

2. Theoretical

We present here briefly the characteristic features of the four models used in this study to account for the same set of experimental data, the GR, the POR, the TD, and the ED models. Although these models are multicomponent models, we limit here their presentation and the discussion of their properties to the single-component case because the experimental data discussed relate only to breakthrough curves of pure BSA.

2.1. The general rate model

We make the following assumptions

(1) The chromatographic process is isothermal.

(2) The mobile phase velocity is constant. The compressibility of the mobile phase is negligible.

(3) The bed is packed with porous particles that are spherical and uniform in size.

(4) The concentration gradient in the radial direction of the bed is negligible.

(5) Local equilibrium exists for each component between the pore surface (monolayer) and the stagnant fluid phase inside the macropores.

(6) The dispersion coefficients are constant.

Based on these assumptions, we write two mass balance equations for each component, one in the mobile phase percolating through the bed of particles, the other inside the particles. The latter involves the stagnant mobile phase and the adsorbed monolayer. Like all models, the GR model is completed by suitable initial and boundary conditions and by the isotherm equation [5,16,18,19].

2.1.1. Mass balance of the ith component in the mobile fluid phase

$$\epsilon_e \cdot \frac{\partial C_i}{\partial t} + u \cdot \frac{\partial C_i}{\partial z} = \epsilon_e D_L \cdot \frac{\partial^2 C_i}{\partial z^2} - (1-\epsilon_e) k_{exp,i} a_p \cdot \left[C_i - C_{p,i}(r = R_p) \right] \quad (1)$$

2.1.2. Mass balance of the ith component in the solid phase

$$\epsilon_p \cdot \frac{\partial C_{p,i}}{\partial t} + (1-\epsilon_p) \cdot \frac{\partial q_i}{\partial t} = D_{eff,i} \cdot \frac{1}{r^2} \cdot \frac{\partial}{\partial r} \left(r^2 \frac{\partial C_{p,i}}{\partial r} \right) \quad (2)$$

2.1.3. Initial conditions

Since we have two partial differential equations, we have one initial condition for each:

$$C_i(0,z) = C_i^0 \quad (3)$$

$$C_{p,i}(0,r,z) = C_{p,i}^0(r,z);\ q_i(0,r,z) = q_i^0(r,z);$$
$$\text{for } 0 < z < L \text{ and } 0 < r < R_p \quad (4)$$

2.1.4. Boundary conditions for Eq. (1)

We have two boundary conditions, one at the column inlet, the other at the column exit. The condition for $t > 0$ and $z = 0$ is:

$$\begin{aligned} u_f C'_{fi} - u(0)C(0) &= -\epsilon_e D_L \cdot \frac{\partial C_i}{\partial z} \\ C'_{fi} &= C_{fi} \quad \text{for } 0 < t < t_p \\ C'_{fi} &= 0 \quad \text{for } t_p < t \end{aligned} \quad (5)$$

The condition for $t > 0$ and $z = L$ is:

$$\frac{\partial C_i}{\partial z} = 0 \quad (6)$$

2.1.5. Boundary conditions for Eq. (2)

There are again two boundary conditions, for $t > 0$ and $r = R_p$:

$$D_{eff} \cdot \frac{\partial C_{p,i}(t,r)}{\partial r} = k_{ext,i} \cdot \left[C_i - C_{p,i}(t,r) \right] \quad (7)$$

and for $t>0$ and $r=0$:

$$\frac{\partial C_{p,i}(t,r)}{\partial r} = 0 \tag{8}$$

Combined with the phase equilibrium isotherm, Eqs. (1)–(8) constitute the mathematical translation of the GR model.

2.2. Lumped pore diffusion model

The POR model is obtained as a simplification of the GR model, as previously explained [20,21]. In this model the mass balances of the ith component in the mobile and the solid phase are written as follows:

$$\epsilon_e \cdot \frac{\partial C_i}{\partial t} + u \cdot \frac{\partial C_i}{\partial z} = \epsilon_e D_L \cdot \frac{\partial^2 C_i}{\partial z^2} - (1-\epsilon_e) k_i a_p \cdot (C_i - \overline{C}_{p,i}) \tag{9}$$

$$\epsilon_p \cdot \frac{\partial \overline{C}_{p,i}}{\partial t} + (1-\epsilon_p) \cdot \frac{\partial \overline{q}_i}{\partial t} = k_i a_p \cdot (C_i - \overline{C}_{p,i}) \tag{10}$$

where $\overline{C}_p$ and $\overline{q}_i$ denote average concentrations. The overall mass transfer coefficient k_i of component i is given by the following relationship:

$$k_i = \left[\frac{1}{k_{ext,i}} + \frac{1}{k_{int,i}} \right]^{-1} \tag{11}$$

where $k_{ext,i}$ and $k_{int,i}$ are the external and the internal mass transfer coefficients, respectively. The internal mass transfer coefficients are calculated from the equations:

$$k_{int,i} = \frac{10 D_{eff,i}}{d_p} \quad D_{eff,i} = \frac{\epsilon_p D_{m,i}}{\gamma} \tag{12}$$

where $D_{m,i}$ is the molecular diffusivity of component i and γ is the tortuosity factor. The initial and the boundary conditions are similar to those used in the GR model.

2.3. The equilibrium–dispersive and the transport–dispersive models

The ED model is easily derived from the POR model, if the term $k_i a_p \cdot (C_i - \overline{C}_{p,i})$ is eliminated from Eqs. (9) and (10). Assuming that the mass transfer resistances are negligible, which is equivalent to the condition $C_i = C_{p,i}$, one can obtain the following form of the mass balance equation for the ED model:

$$\epsilon_T \cdot \frac{\partial C_i}{\partial t} + (1-\epsilon_T) \cdot \frac{\partial q_i}{\partial t} + u \cdot \frac{\partial C_i}{\partial z} = \epsilon_e D_L \cdot \frac{\partial^2 C_i}{\partial z^2} \tag{13}$$

This form is similar to the one found in the classical literature [3]. The only difference is in the replacement of the total porosity in the right-hand-side of Eq. (13) by the external porosity.

The initial and boundary conditions are adapted from those used in the GR model. As in all the models, q_i is calculated from the appropriate isotherm equation.

In cases in which the mass transfer resistances, without being large, cannot be entirely neglected, the TD model is frequently used [6–15]. This model consists in Eq. (13) completed by the following kinetic equation:

$$\frac{\partial q_i}{\partial t} = k_{f,i} \cdot (q_i^* - q_i) \tag{14}$$

where q_i^* is the concentration in the adsorption monolayer at the adsorbent surface in equilibrium with the concentration C_i in the mobile phase.

2.4. Basis of a comparison between the GR, POR, and TD models

As will be demonstrated by a comparison between experimental breakthrough curves and those calculated using the different models discussed above, the TD model does not account correctly for the experimental data (see Section 3.1). In fact, the TD model should not be used to model the chromatography process studied [17]. As explained in the Introduction, conditions for the selection of the most suitable model, depending on the rate of the mass transfer kinetics, were previously established for the GR, the POR and the ED models [16]. These conditions were derived for high concentration chromatography, in the case of a Langmuir isotherm. We now discuss their extension to the TD model which was left out from this earlier analysis. To perform such a comparison between models that are so different, it is convenient to rewrite all of them under dimensionless form.

2.4.1. Dimensionless form of the GR, the POR, the TD, and the ED models

The dimensionless variables used here are the following:

$$x=\frac{z}{L} \qquad \tau=\frac{tu}{L\epsilon_e} \qquad R=\frac{r}{R_p}$$
$$y_i=\frac{C_i}{C_r} \qquad y_{p,i}=\frac{C_{p,i}}{C_r} \qquad Q_i=\frac{q_i}{C_r} \tag{15}$$
$$\mathrm{Pe}=\frac{ud_p}{D_L\epsilon_e} \quad \mathrm{St}_i=\frac{k_{ext,i}a_pL\epsilon_e}{u} \quad \mathrm{Bi}=\frac{k_{ext}R_p}{D_{eff}}$$

where C_r is a reference concentration which we will take here as equal to the feed concentration of the injected sample, C_f.

Now, the two mass balance equations of the GR model (Eqs. (1) and (2)) can be rewritten as follows:

$$\frac{\partial y_i}{\partial\tau}+\frac{\partial y_i}{\partial x}=\frac{1}{\mathrm{Pe}}\cdot\frac{\partial^2 y_i}{\partial x^2}-\frac{(1-\epsilon_e)}{\epsilon_e}\cdot\mathrm{St}_i \cdot\left[y_i-y_{p,i}(R=1)\right] \tag{16}$$

$$\epsilon_p\cdot\frac{\partial y_{p,i}}{\partial\tau}+(1-\epsilon_p)\cdot\frac{\partial Q_i}{\partial\tau}=\frac{\mathrm{St}_i}{3\mathrm{Bi}_i}\cdot\frac{1}{R^2}\cdot\frac{\partial}{\partial R}\cdot\left(R^2\cdot\frac{\partial y_{p,i}}{\partial R}\right) \tag{17}$$

The initial conditions (at $\tau=0$) are:

$$\begin{aligned} &y_i(0,x)=y_i^0 && \text{for } 0<x<1\\ &y_{p,i}(0,R,x)=y_{p,i}^0(R,x)\}\\ &Q_i(0,R,x)=Q_i^0(R,x)\} && \text{for } 0<x<1;\ 0<R<1 \end{aligned} \tag{18}$$

The boundary conditions of the first mass balance equation are:

$$\text{For } \tau>0;\ x=0 \quad y'_{f,i}-y_i(\tau,0)=-\frac{1}{\mathrm{Pe}}\cdot\frac{\partial y_i(\tau,0)}{\partial x},$$

with $y'_{f,i}=y_{f,i}$ for $\tau\in[0,\tau_p]$

and with $y'_{f,i}=0$ for $\tau>\tau_p$

$$\text{For } \tau>0;\ x=1 \quad \frac{\partial y_i(\tau,1)}{\partial x}=0 \tag{19}$$

The boundary conditions of the second mass balance equation are:

$$\text{For } \tau>0,\ R=1\ \frac{\partial y_{p,i}(\tau,R)}{\partial R}=\mathrm{Bi}_i\cdot[y_i-y_{p,i}(\tau,R)]$$
$$\text{For } \tau>0,\ R=0\ \frac{\partial y_{p,i}(\tau,R)}{\partial R}=0 \tag{20}$$

With the same dimensionless variables the POR model can be rewritten as follows:

$$\frac{\partial y_i}{\partial\tau}+\frac{\partial y_i}{\partial x}=\frac{1}{\mathrm{Pe}}\cdot\frac{\partial^2 y_i}{\partial x^2}-\frac{1-\epsilon_e}{\epsilon_e}\cdot\mathrm{St}'_i\cdot(y_i-\bar{y}_{p,i}) \tag{21}$$

$$\epsilon_p\cdot\frac{\partial\bar{y}_{p,i}}{\partial\tau}+(1-\epsilon_p)\cdot\frac{\partial\overline{Q}_i}{\partial\tau}=\mathrm{St}'_i\cdot(y_i-\bar{y}_{p,i}) \tag{22}$$

$$\mathrm{St}'_i=\frac{\mathrm{St}_i}{1+\mathrm{Bi}_i/5}=\frac{k_ia_pL\epsilon_e}{u} \tag{23}$$

This model has initial and boundary conditions that are similar to those of the GR model.

The dimensionless mass balance equation of the ED model is given by:

$$\epsilon_T\cdot\frac{\partial y_i}{\partial\tau}+(1-\epsilon_T)\cdot\frac{\partial Q_i}{\partial\tau}+\epsilon_e\cdot\frac{\partial y_i}{\partial x}=\epsilon_e\cdot\frac{1}{\mathrm{Pe}}\cdot\frac{\partial^2 y_i}{\partial x^2} \tag{24}$$

Finally, the dimensionless form of the TD model consists in the previous mass balance equation and in the following kinetic equation:

$$\frac{\partial Q_i}{\partial\tau}=\mathrm{St}''_i\cdot(Q_i^*-Q_i) \quad \text{with } \mathrm{St}''_i=\frac{k_{f,i}L\epsilon_e}{u} \tag{25}$$

The initial and boundary conditions of these last two models are similar to those of the GR model.

2.4.2. Numerical calculations of solutions of the POR, TD, and ED models

The first criterion previously established [16] and cited in the Introduction regards the equivalence of the solutions of the GR and the POR model. It states that if $\mathrm{Pe}>100$ and $\mathrm{St}/\mathrm{Bi}>5$, there are no significant differences between the solutions of these two models. This condition is valid for any isotherm, including a linear one. It will be verified in the calculations of all the solutions discussed later.

In the calculations made to compare the elution profiles obtained with the different models com-

pared, we assumed that the retention behavior of the compound considered follows Langmuir isotherm behavior, with $a_1=8$, $b_1=4$ for its two numerical coefficients. The total column porosity, the external porosity of the packing, and the particle or internal porosity were assumed to be equal 0.75, 0.375, and 0.60, respectively (the internal porosity being the total pore volume reported to the volume of the particles, not that of the column as it is some times done). The relevant values of the dimensionless Peclet (Pe) and Stanton numbers (St′ or St″) are given in the figure captions.

In all the following discussions, we will consider that the band profiles calculated as solutions of two different models are practically identical when the relative difference of their second central moments ($\Delta\mu_2/\mu_2$) is less than 2% and the relative difference of their numbers of theoretical plates ($\Delta N/N$) is less than 4% (the number of theoretical plates being derived using the moment method [3]).

3. Experimental

In this work, we reevaluate, on the basis of the GR and the POR models, experimental data on the mass transfer kinetics of BSA in anion-exchange chromatography previously discussed [6,17]. These data were initially interpreted using the TD model after it was shown that the ED model was not applicable. We supply here only the brief review of the experimental conditions which is necessary to understand the results derived in this paper. Further details on the experimental work can be found in the original papers [6,17].

3.1. Experimental conditions

The experiments were performed using a 7.5× 0.75 cm stainless steel column (No. S0116) packed with TSK-GEL-DEAE-5PW (average particle size, 10 μm; average pore size, 1000 Å) from Tosohaas (Montgomeryville, PA, USA). The column had a hold-up volume of 2.58 ml, contained a volume of packing material of 0.73 ml, and had an efficiency of 2800 theoretical plates for cytidine-5′-monophosphate (unretained) at a flow-rate of 1 ml min^{-1} of an eluent containing 35 m*M* NaCl in a 20 m*M* Tris–HCl buffer (pH 8.0). The total porosity of the column was $\epsilon_T=0.779$. The external porosity of this column was not measured but estimated at $\epsilon_e=0.375$. From the values of ϵ_T and ϵ_e, the porosity of the particles is estimated at $\epsilon_p=0.646$. It should be noted that any error made in the estimate of the external porosity has a slight influence on the estimate of the diffusion coefficient but nearly none on the final results of this work. The mobile phase was a buffer solution prepared by dissolving either 25 m*M* Bis-Tris or 50 m*M* Tris in water and titrating with HCl until pH 6.0. The sample solutions were prepared by dissolving known amounts of BSA in these buffer solutions.

3.2. Procedures for the determination of the isotherm and rate coefficients

Equilibrium data were obtained by frontal analysis [3,22]. After a breakthrough had been acquired, a new, more concentrated, buffer solution of BSA was pumped into the column until the concentration front broke through. This solution was obtained by mixing the pure mobile phase and a solution of BSA in the mobile phase, using the step function of the solvent delivery system. A series of such single breakthrough curves were measured, in the order of increasing steps of BSA concentration. After completion of each series of experiment, the column was regenerated, following a standard procedure, then reequilibrated with the mobile phase [17]. The flow-rate was 1 ml min^{-1}. The amount of BSA adsorbed by the stationary phase at equilibrium was derived from the retention volume of the half-height of the breakthrough curve, through the classical equation [22]:

$$q^* = \frac{C_p \cdot (V_F - V_0)}{V_s} \tag{26}$$

where q^* is the amount adsorbed on the solid phase when it reaches equilibrium with the concentration C_p in the fluid phase, V_F is the retention volume of the half-height of the breakthrough curve, V_0 is the column hold-up volume, and V_s is the volume of adsorbent in the column. The isotherm data were fitted to a modified bi-Langmuir isotherm equation

that gave a better fit than either a simple Langmuir or a bi-Langmuir isotherm model:

$$q = \frac{a_1 C}{1 + b_1 C} + a_2 C \tag{27}$$

Using the best equilibrium isotherm and the TD model to calculate breakthrough profiles, the best values of k_f were estimated for each concentration step, by minimizing the difference between the experimental and the calculated profiles. Minor adjustments had to be made in same cases for minor changes in the retention times of certain experimental breakthrough curves [17].

3.3. Procedures for the estimation of the other numerical parameters

In the case of the GR model used in this work, the value of the external mass transfer rate coefficient were calculated from the Wilson–Geankoplis correlation [23]:

$$\mathrm{Sh} = \frac{k_{ext} d_p}{D_m} = \frac{1.09}{\epsilon_e} \cdot \mathrm{Sc}^{1/3} \mathrm{Re}^{1/3} \tag{28}$$

where Sh, Sc, and Re are the Sherwood, the Schmidt, and the Reynolds numbers, respectively. This gives $k_{ext} = 0.42$ cm s^{-1}.

The molecular diffusivity, D_m, was derived from the following correlation cited in Ref. [3]:

$$D_{m,B} = 8.31 \cdot 10^{-8} \cdot \frac{T}{\eta_{sv} M_B^{1/3}} \tag{29}$$

where the subscripts B and sv stand for BSA and the solvent, respectively. A diffusivity of $3.6 \cdot 10^{-5}$ cm^2 min^{-1} was obtained.

The axial dispersion coefficient was calculated from the relationship $Pe = 2N$ and found equal to 0.00807 cm^2 min^{-1}, since the contributions of axial and eddy diffusions are the same for the unretained compound and for BSA.

Finally, the tortuosity factor, γ, was derived from the relationship [3]:

$$\gamma = \frac{(2 - \epsilon_p)^2}{\epsilon_p} \tag{30}$$

The values of the diffusion coefficient, the external mass transfer coefficient, and the axial dispersion coefficients so obtained were used for all calculations made with either the GR or the POR models. The calculations of breakthrough curves were performed using the same values of the external mass transfer coefficient, k_{ext}, and the dispersion coefficient, D_L, (equal to 0.42 cm s^{-1} and 0.00807 cm^2 min^{-1}, respectively) in all models.

3.4. Programming and CPU times

The programs used to perform all the numerical calculations discussed in this work were written using the method of orthogonal collocation on finite elements [3–5]. The calculations of numerical solutions of sophisticated models such as the GR and the POR models required one to two orders of magnitude longer CPU run times than those of simple models like the TD or the ED models when these models are solved using programs based on the Rouchon algorithm [3,24]. However, a Rouchon-like algorithm was developed for the POR model [25]. However, finite difference based programs were not used in the present case. The need for these less accurate algorithms in the calculation of band profiles has become less critical in recent years. In this work, for example, the typical computing times on a recent Pentium III-based desk computer for the numerical calculations regarding the reevaluation of the BSA breakthrough curves required usually 2 to 3 min with the POR model and between 3 and 30 min with the GR model.

4. Results and discussion

4.1. Band profiles of BSA obtained with the TD model

The best values of the numerical parameters a_1, a_2, b_2 in Eq. (27) and a selection of best values of the external mass transfer coefficient, k_f, for three different concentration steps are listed in Table 1. Fig. 1 shows two experimental breakthrough curves obtained at pH 7.5, those corresponding to the lowest and the largest concentration steps. This figure also illustrates the fitting method used to estimate k_f with the TD model. The experimental data for the step

Table 1
Parameters of the equilibrium isotherm and the overall mass transfer coefficient

	pH 7.5	pH 6.0
a_1 (–)	3040	1380
b_1 (ml mg^{-1})	32.1	17.3
a_2 (–)	3.38	11.9
k_f (min^{-1})	0.08 at $C=0.167$	0.11 at $C=0.156$
	0.50 at $C=1.41$	0.38 at $C=0.90$
	1.22 at $C=2.77$	1.01 at $C=2.78$

concentration $C=2.77$ mg ml^{-1} (Fig. 1b) were well accounted for with a rate coefficient $k_f=1.22$ min^{-1}. Neither this rate coefficient nor the value $k_f=0.5$ min^{-1}, which was the best estimate of k_f for $C=$ 1.41 mg ml^{-1}, could be used properly to fit the experimental data for the concentration step $C=$ 0.167 mg ml^{-1} (Fig. 1a). Similar results (not shown) were obtained at pH 6.0.

These results demonstrate a dependence of the overall mass transfer rate coefficient on the BSA concentration [17]. They could arise either from an actual concentration dependence of the external mass transfer and/or the internal mass transfer resistances or from a model error resulting from the necessary compromises made in forcing too simple a model onto the experimental data. Thus, the goal of this work is to investigate whether this dependence is real or apparent.

4.2. Band profiles of BSA obtained with the GR model

The numerical calculation of breakthrough curves using the GR model with the effective molecular diffusion coefficient derived from the correlation suggested by Tsou and Graham [26], Eq. (29), gives too steep adsorption fronts. In the following, we used for the molecular diffusivity inside the pores of the adsorbent an estimate derived by fitting to the GR model the experimental data [6] for the largest concentration step ($C=2.766$ mg ml^{-1}), at pH 7.5. The value obtained was $D_m=1.22\cdot10^{-6}$ cm^2 min^{-1}. This value was used in all the calculations discussed in the following. The value of the effective diffusion coefficient derived from Eq. (12) is $3.6\cdot10^{-5}$ cm^2 min^{-1}. Accordingly, the estimate of the diffusion coefficient of BSA in the pores of the resin is about 30 times smaller than its bulk value obtained from Eq. (29). A similar conclusion was reported previously by several groups. Graham and Fook [27] studied the equilibrium and the kinetics of adsorption of BSA on a DEAE-resin by a batch method. They reported that the diffusion coefficient in the resin was about 100 times smaller than that in the bulk phase. Similarly Tsou and Graham [26] reported a calculated effective particle diffusivity of BSA in DEAE-Sephadex A-50 about 20 times smaller than the bulk diffusivity. Skidmore et al. [28] determined the

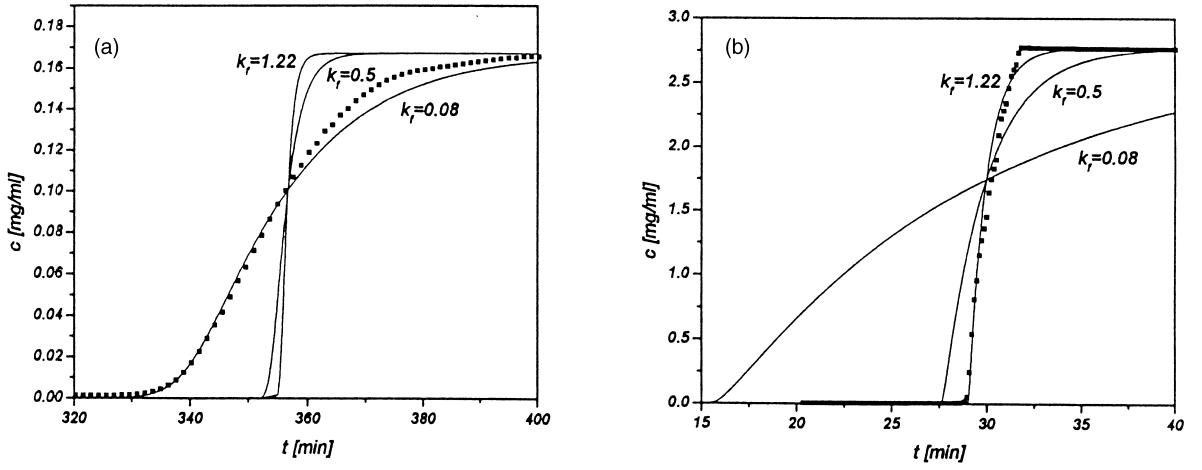

Fig. 1. Comparison between the experimental breakthrough curves (symbols) and numerical solutions (solid lines) of the TD model for different values of the mass transfer rate coefficient (see Table 1). These numerical values give the best fit of the experimental data [6] to the model for concentration steps equal to 0.167 (a, left), 1.411 (not shown), and 2.766 (b, right) mg ml^{-1}, respectively.

characteristics of the equilibrium and the kinetics of the adsorption of BSA and lysozyme on the strong cation exchanger S Sepharose FF and reported a value of the effective particle diffusivity of $5.1 \cdot 10^{-6}$ cm^2 min^{-1}. Fernandez and Carta [29] and Fernandez et al. [30] reported values of $5.5 \cdot 10^{-7}$ cm^2 min^{-1} for the intraparticle diffusion coefficient of BSA. These values were obtained assuming that the driving force for diffusion through the particles of a composite silica–polyacrylamide gel anion exchanger is the total BSA concentration. Yoshida et al. [31] investigated the mass transfer of BSA on a strongly basic adsorbent, chitosan, using the shallow bed adsorption method. They reported values of $6 \cdot 10^{-8}$ and $2.7 \cdot 10^{-7}$ cm^2 min^{-1} for the intraparticle diffusion coefficient of BSA, assuming that the total BSA concentration is the driving force of diffusion.

Fig. 2a–c show typical comparisons between the experimental breakthrough curves at pH 7.5 and the profiles calculated as numerical solutions of the GR model.

It is important to observe that, although all the numerical calculations were performed with the same set of numerical coefficients for the isotherm and all the kinetic coefficients, all the numerical solutions closely approximate the experimental curves.

No dependence of any of the diffusion or rate coefficients on the concentration needs to be intro-

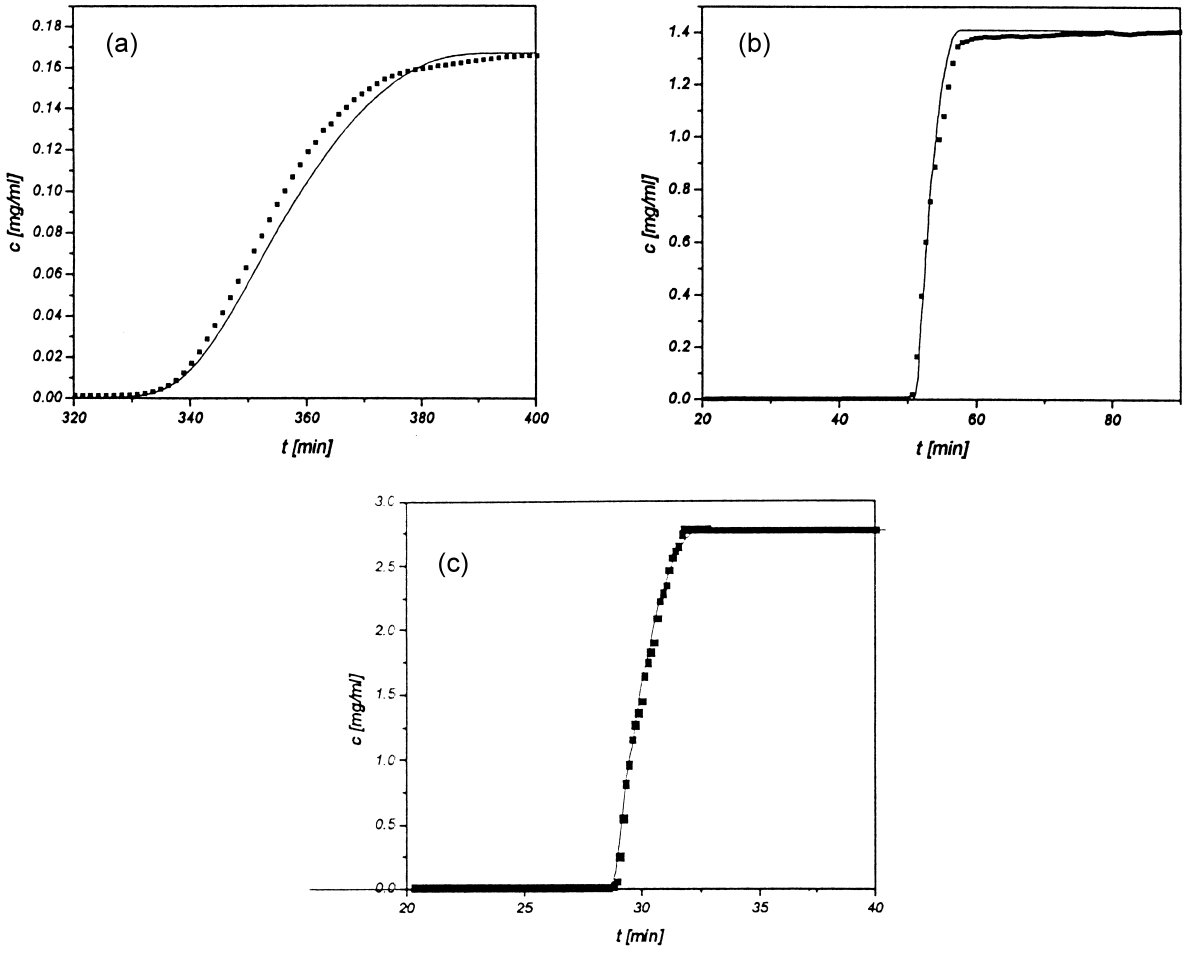

Fig. 2. Comparison between an experimental breakthrough curve (symbols) and the numerical solution (solid lines) of the GR model. Experimental conditions: (a) pH 7.5, concentration step, $C = 0.167$ mg ml^{-1}. (b) pH 7.5, concentration step, $C = 1.411$ mg ml^{-1}. (c) pH 7.5, concentration step, $C = 2.766$ mg ml^{-1}. All calculations were made with Pe = 2, $N = 5600$, Bi = 749, St = 3106.

duced to observe this agreement in the whole range of concentration investigated. Similar conclusions can be derived from the comparison of the experimental data and the profiles calculated at pH 6.0, as illustrated in Fig. 3.

4.3. Band profiles of BSA obtained with the POR model

The results obtained with the POR model are illustrated in Fig. 4 (pH 7.5). As in the case of the GR model, the calculations of the three breakthrough profiles in Fig. 4 were carried out using the same set of numerical coefficients. No dependence of the coefficients of the mass transfer resistances on the concentration is needed.

The agreement between the experimental and the calculated breakthrough curves is better for the solutions of the GR model than for those of the POR model. This is not surprising because, in this case the ratio St/Bi is equal to 4.1 and, as indicated earlier, the POR model should not be used in this case [16].

4.4. General comments on the calculations of the band profiles of BSA

Breakthrough curves that practically cannot be distinguished from each other were obtained whether the external mass transfer resistances and the axial dispersion in the mobile phase stream were ignored or not (not shown). So, in the present case (BSA on TSK-GEL-DEAE-5PW anion exchanger), only the mass transfer resistance inside and across the adsorbent particles must be taken into account. This explains why the TD model fails properly to account for the experimental results. This model cannot properly take internal mass transfer into account.

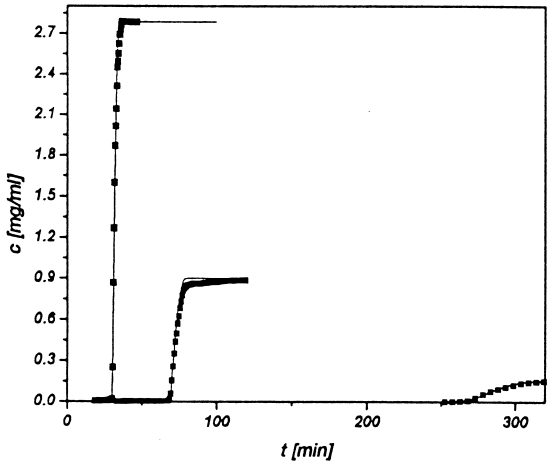

Fig. 3. Comparison between experimental breakthrough curves (symbols) and numerical solutions (solid lines) of the GR model. Experimental conditions: pH 6.0, concentration steps, $C=2.783$, 0.899, and 0.156 mg ml^{-1}.

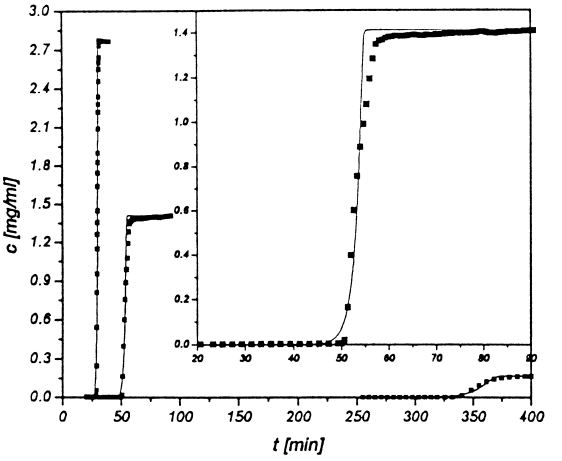

Fig. 4. Comparison between experimental breakthrough curves (symbols) and numerical solutions (solid lines) of the POR model. Experimental conditions: pH 7.5, concentration steps, $C=2.766$, 1.411, and 0.167 mg ml^{-1}. The inset is for $C=1.411$ [mg ml]$^{-1}$.

4.5. Comparison between profiles calculated with the POR, TD, and ED models

Before discussing the results of these calculations, we must notice that a comparison of the definitions of the numbers St″ and St′ suggests that the relationship $ka_p=k_f$ should hold. It cannot be exact, however, because, at the difference with the ED model, the TD model cannot be derived from the POR model and, in general, a solution of the TD model and one of the POR model with St″=St′ and the same Peclet number will be different. However, at the first attempt we will check if, for a given Peclet number, there exists a couple of Stanton numbers St″=St′ for which the solution of the TD model and that of the POR model cannot be distinguished.

Figs. 5–8 compare the solutions calculated with the POR, the TD, and the ED models for Pe=10 000

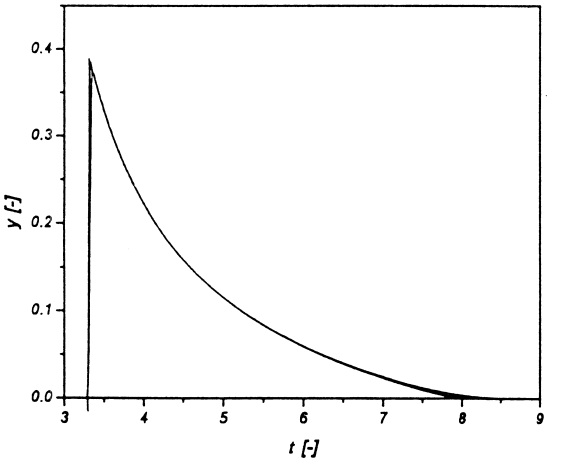

Fig. 5. Comparison between the solutions of the POR, the TD and the ED models for Pe = 10 000, St′ = St″ = 500, $C_f = 1$, and $\tau_p = 0.5$. All three lines coincide for all practical purposes.

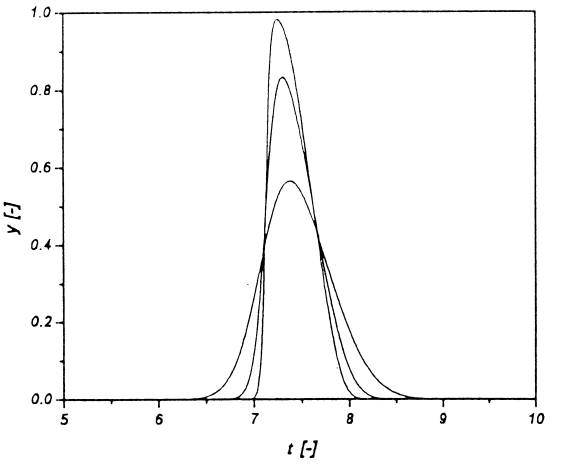

Fig. 7. Same as Fig. 5 except $C_f = 0.01$ ($b_1 C_f = 0.04$; in the range between 0 and 0.01, the isotherm is barely different from its initial tangent).

and St′ = St″ = 500, for different values of the sample size, defined as the product of the sample concentration, C_f, the flow-rate, and the duration of the rectangular injection, t_p.

At high concentrations ($C_f = 1$ and impulse time $\tau_p = 0.5$, Fig. 5), the column is strongly overloaded (note that the product $b_1 C_f$, that characterizes the deviation of the isotherm, Eq. (27), is equal to 4) and all three models give practically the same elution curves. For $C_f = 0.1$ ($b_1 C_f = 0.4$, Fig. 6), the solutions obtained with the TD and the ED models differ too much from that of the POR model, being much steeper, to be acceptable as actual solutions of the problem. At this concentration, however, all the band profiles coincide for St′ = St″ > ca. 4000. Decreasing the concentration to $C_f = 0.01$ (Fig. 7) and $C_f = 0.001$ (Fig. 8) leads to a practically linear problem. It is known that at low concentrations, the deviation of the isotherm from linear behavior is proportional to the product $b_1 C_f$ in Eq. (27) and that the deviation of band profiles from those obtained in the linear case is

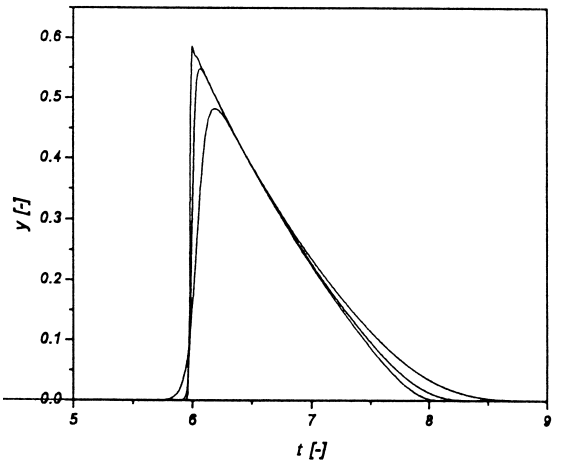

Fig. 6. Same as Fig. 5, except $C_f = 0.1$. The highest line is the solution of the ED model, the medium line, that of the TD model, and the lowest line, that of the POR model.

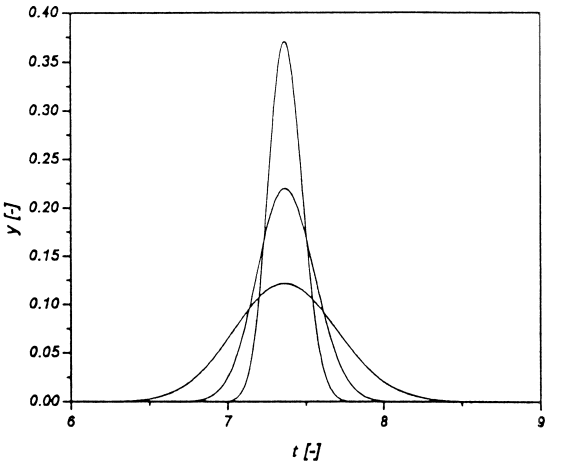

Fig. 8. Same as Fig. 5 except $C_f = 0.001$, and $\tau_p = 0.1$ ($b_1 C_f = 0.004$ corresponds to a linear isotherm).

small for $b_1C_f<0.05$ and negligible for $b_1C_f<0.01$ [3]. However, the differences between the band profiles calculated with the three models increase with decreasing concentrations. The profiles obtained for Pe = 10 000 and these two concentrations become nearly identical for values of $St' = St''$ equal to ca. 10 000 and 80 000, respectively. Those are high values, corresponding to fast mass transfers and high column efficiency.

Similar results were obtained for smaller values of the Peclet number. The differences between the numerical solutions of the three models decrease with decreasing Peclet number (Fig. 9) but they still remain clearly visible for values of the Peclet number as small as 100 (Fig. 10).

4.6. General comments on the results of comparisons between calculated band profiles

It might be surprising that we conclude to the superiority of the results obtained with the GR model when it has been abundantly demonstrated that the ED model gives satisfactory or excellent results under either nonlinear or linear conditions [3]. The origin of the differences observed in Figs. 7–10 between the profiles calculated at low concentrations, under linear or quasi-linear conditions, is in the assumptions made regarding the way the mass transfer resistances are accounted for. In this work, we stuck to the original definition of the ED model. Only the axial and eddy diffusions are accounted for. Mass transfer between phases is assumed to be infinitely fast.

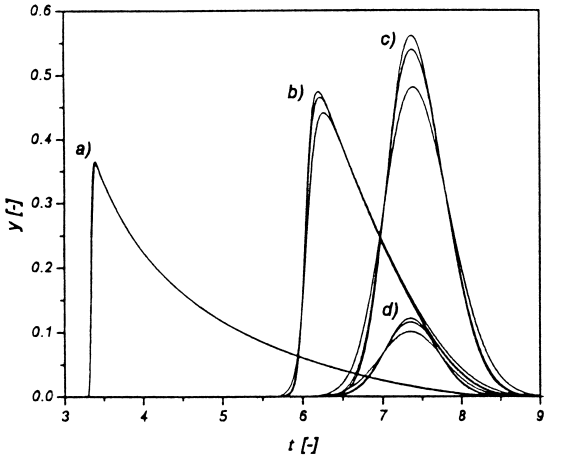

Fig. 9. Comparison between the solutions of the POR, the TD, and the ED models for Pe = 1000, $St' = St'' = 1000$. In each case, the highest line is for the ED model, the central one for the TD model, and the lowest for the POR model. (a) $C_f = 1$, $\tau_p = 0.5$, (b) $C_f = 0.1$, $\tau_p = 0.5$, (c) $C_f = 0.01$, $\tau_p = 0.5$, (d) $C_f = 0.001$, $\tau_p = 0.1$.

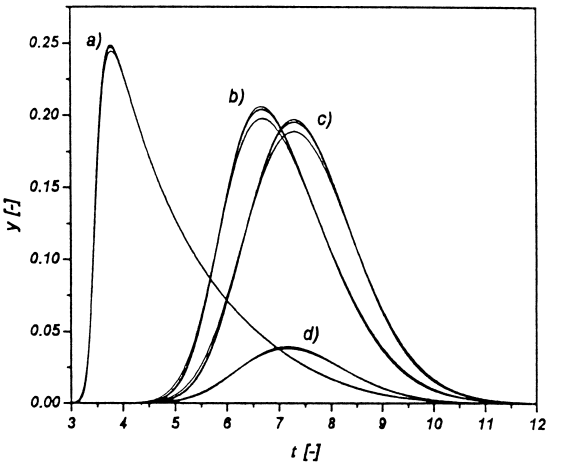

Fig. 10. Comparison between the solutions of the POR, the TD, and the ED models for Pe = 100, $St' = St'' = 500$. (a) $C_f = 1$, $\tau_p = 0.5$, (b) $C_f = 0.1$, $\tau_p = 0.5$, (c) $C_f = 0.01$, $\tau_p = 0.5$, (d) $C_f = 0.001$, $\tau_p = 0.1$.

Furthermore, the numerical calculations were carried out using a program based on collocation on finite elements, not on finite differences such as the Rouchon–Golshan method [3]. With collocation on finite elements, there is no numerical diffusion and it is pointless to try and relate the space increment to the column height equivalent to a theoretical plate (HETP). This explains entirely the differences between the profiles derived from the GR and the ED models in Figs. 7–10. If a conventional finite difference program were used with integration increments derived as is now conventional [3], the band profiles obtained with the GR and the ED models would be the same at infinite dilution. There would still be differences at high concentrations because numerical errors due to the approximations made by the algorithm are larger with finite differences [3].

In each of the cases illustrated above, we observed that nearly identical solutions are afforded by the TD and the ED models for smaller values of $St'' = St'$ than are required to achieve the same result for solutions of the TD and the POR models. From this

observation, it follows that when the solutions of the TD and the POR models are close enough to be considered as identical in a concentration interval 0 to C, the solutions of the ED model are also identical to those of the POR model. The conditions required for the equivalence of the solutions of the TD and POR model are the same as those for the equivalence of the ED and POR models previously derived [16]. Therefore, the use of the TD model is rarely justified.

Using the criterion adopted earlier for the equivalence of the solution of two models (relative difference of their second central moments less than 2% and that of their numbers of theoretical plates less than 4%), we found from numerous calculations carried out under a variety of numerical conditions that the solutions of the ED, the TD and the POR models are practically identical when the following conditions are fulfilled:

(1) For Pe$>$10 000: St$'$=St$''>$80 000.
(2) For Pe$>$1000: St$'$=St$''>$10 000.
(3) For Pe$>$500: St$'$=St$''>$4000.
(4) For Pe$>$100: St$'$=St$''>$2000.

Note that the minimum Stanton number required for peak profile equivalence decreases rapidly with decreasing Peclet number because, in the same time, the corresponding profiles become broader. The peaks showed in Fig. 11 fulfill the conditions above. The relative differences between the second centered moments and the efficiencies of the peaks obtained with the TD and the POR models and shown in the figure are 2.1% and 4%, respectively.

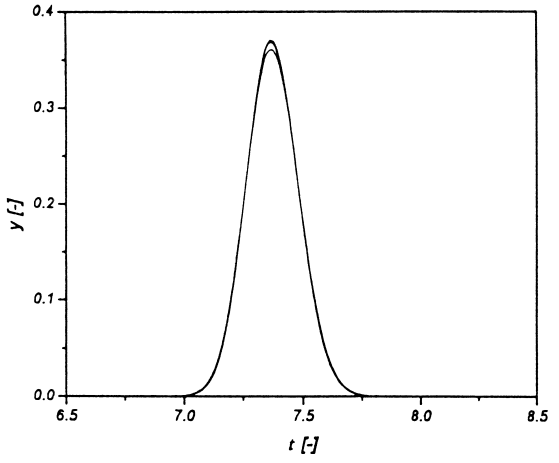

Fig. 11. Comparison between the solutions of the POR, the TD and the ED models for Pe=10 000, St$'$=St$''$=80 000, C_f=0.001, and τ_p=0.1.

The result that we just obtained is trivial. The TD model becomes equivalent to the POR model (and to the ED model) when the mass transfer resistances can be neglected at the Peclet number considered. However, the band profiles calculated with the TD model can be equivalent to those obtained with the POR model for a properly chosen value of St$''$. For example, for Pe=10 000 and St$'$=500, these profiles are equivalent for St$''$=130 at C_f=0.1, for St$''$=115 at C_f=0.01, and for St$''$=110 at C_f=0.001. In other words, we must use a markedly lower value of the Stanton number, hence of the rate coefficient, than used with the POR model and the overall mass transfer coefficient, k_f, must be increased with increasing concentration if the profiles calculated with the TD model are to be equivalent to those calculated with the POR model. Moreover, the value of St$''$ giving TD profiles equivalent to POR profiles obtained with a given value of St$'$ depends not only on the concentration but also on the isotherm parameters. For example, for Pe=10 000, St$'$=500, C_f=0.1, τ_p=0.5, a_1=4, b_1=2, St$''$ should be equal to 185 while for a_1=8, b_1=4, it should be 130, as was stated above. Under these conditions, the TD model becomes an empirical method of fitting band profiles but the numerical parameters obtained have little physical meaning.

4.7. Analysis of the conditions of equivalence of the TD and POR models

The results discussed in the previous section demonstrate that equivalence between the solutions of the TD and the POR models calculated for a given set of experimental conditions in a range of sample sizes cannot be achieved unless the Stanton number of the TD model is considered to be a function of the concentration and of the isotherm coefficients. A relationship between the Stanton numbers of the POR and TD models, St$'$ and St$''$, respectively, can be derived by considering the Van Deemter equation [32]:

$$H = \frac{2D_L\varepsilon_T}{u} + 2\cdot\left(\frac{k_0'}{1+k_0'}\right)^2\cdot\frac{u}{\varepsilon_T k_0' k_f} \quad (31)$$

itself a simplification of the analytical solution of the

TD model derived by Lapidus and Amundson [33] in the case of a relatively high column efficiency: a similar equation was derived by Kucera [34] for the GR model:

$$H = \frac{2D_L\epsilon_e}{u} + 2\cdot\left(\frac{k_1}{1+k_1}\right)^2 \cdot\left[\frac{ud_p^2}{60F'\epsilon_e D_{eff}} + \frac{ud_p}{6F'\epsilon_e k_{ext}} + \left(\frac{k_p}{1+k_p}\right)^2\cdot\frac{u}{F'k_a\epsilon_e}\right] \quad (32)$$

and we have the following relationships between the parameters involved:

$$k_0' = Fa \qquad k_1 = F'\cdot\left[\epsilon_p + (1-\epsilon_p)a\right]$$
$$k_p = \frac{1-\epsilon_p}{\epsilon_p}\cdot a \quad F = \frac{1-\epsilon_T}{\epsilon_T} \quad F' = \frac{1-\epsilon_e}{\epsilon_e} \quad (33)$$

where a is the slope of the linear isotherm. We will assume that the kinetics of adsorption/desorption is infinitely fast ($k_a \approx \infty$) and neglect the third term in the square bracket of the right-hand-side of Eq. (32). We will also assume that, in the case of a nonlinear isotherm, the rate coefficient k_1 is given by the following relationship:

$$k_1 = F'\cdot\left[\epsilon_p + (1-\epsilon_p)\cdot\frac{\Delta Q}{\Delta C}\right] \quad (34)$$

where $\Delta Q/\Delta C$ is the slope of the isotherm chord at the local concentration. For consistency, the retention factor was taken as:

$$k_0' = F\cdot\frac{\Delta Q}{\Delta C} \quad (35)$$

Finally, note that Eq. (31) was derived as a solution of the following mass balance equation:

$$\epsilon_T\frac{\partial C_i}{\partial t} + (1-\epsilon_T)\cdot\frac{\partial q_i}{\partial t} + u_f\cdot\frac{\partial C_i}{\partial z} = \epsilon_T D_L\cdot\frac{\partial^2 C_i}{\partial z^2} \quad (36)$$

while in this work we prefer to write the mass balance as in Eq. (13). Then, the Van Deemter equation should rather be rewritten:

$$H = \frac{2D_L\varepsilon_e}{u} + 2\cdot\left(\frac{k_0'}{1+k_0'}\right)^2\cdot\frac{u}{\varepsilon_T k_0' k_f} \quad (37)$$

Now, identifying the two plate height equations, we can derive the following relationship between their parameters:

$$k_f = \frac{F'ka_p\epsilon_e\left(\frac{k_0'}{1+k_0'}\right)^2}{k_0'\epsilon_T\cdot\left(\frac{k_1}{1+k_1}\right)^2} \quad (38)$$

or

$$St'' = \frac{F'\epsilon_e\cdot\left(\frac{k_0'}{1+k_0'}\right)^2}{k_0'\epsilon_T\cdot\left(\frac{k_1}{1+k_1}\right)^2}\cdot St' = \frac{F'\epsilon_e}{\epsilon_T}\cdot\frac{k_0'(1+k_1)^2}{k_1^2(1+k_0')^2}\cdot St' \quad (39)$$

Eq. (38) shows that the apparent rate coefficient of the TD model increases with increasing concentration, since $\Delta Q/\Delta C$, hence k_1 and k_0' decrease with increasing concentration in the general case in which the equilibrium isotherm is convex upward (e.g., Langmuir isotherm). This prevision agrees well with all the results discussed earlier in this work.

The agreement between the solutions of the POR and the TD models calculated with the value of St″ derived from Eqs. (34), (35), and (39), for experimental conditions that are typical of current chromatographic applications, is excellent, as illustrated in Fig. 12. The same agreement was obtained for other isotherms, such like Toth, the Langmuir–Freundlich and even for an S-shaped isotherm (not shown). However, for small Stanton numbers (see Fig. 13), or for combinations of small Peclet and Stanton numbers (see Fig. 14), a small discrepancy between the solutions of the POR and the TD models begins to become noticeable.

5. Conclusion

A reevaluation of previous experimental data on the mass transfer kinetics of BSA in anion-exchange chromatography under nonlinear conditions was made using the general rate model and the pore diffusion model of chromatography. The results obtained show that the contributions to band broadening of the external mass transfer resistances

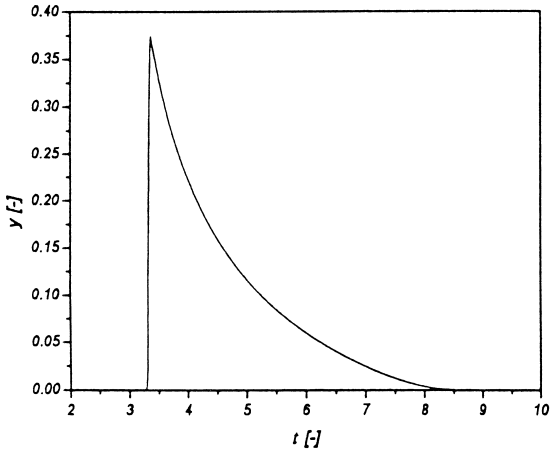

Fig. 12. Comparison between the solutions of the POR and the TD models for Pe = 2000, St′ = 1000, $C_f = 1$, and $\tau_p = 0.5$. The St″ value was calculated from Eqs. (34), (35) and (39), relating it to the local concentration. The two lines practically coincide everywhere.

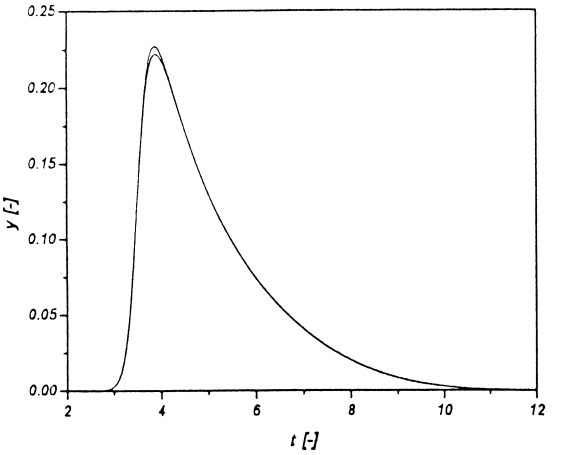

Fig. 14. Same as in Fig. 12 but Pe = 100, St′ = 100. The upper line is the solution of the POR model, the lower line that of the TD model.

and of axial dispersion could be ignored in an accurate description of the behavior of BSA. The band broadening observed is controlled by the mass transfer resistances taking place inside the pores of the adsorbent particles. The rate coefficients of these contributions do not depend on the concentration in the whole range studied when their values are estimated with the GR model.

By contrast, the use of too simple a model, such as the transport–dispersive model, to analyze chromatographic data can lead to erroneous conclusions caused by the model errors that arise during the process of fitting the experimental data to the profiles generated by the model. The transport–dispersive model can be used for modeling column chromatography processes only if the overall mass transfer coefficient or the Stanton number are calculated using Eqs. (38) or (39), respectively. Although excellent description of band profiles can be obtained with the TD model, the rate coefficient derived from a fitting of the data to this model do not have the simple physical meaning that is usually attributed to it.

Applying the POR model requires knowledge of the external mass transfer resistances, the external and the internal diffusion coefficients, and of the tortuosity factor while calculations with the TD model require only that the overall mass transfer coefficient be known. However, when the determination of exact values of k_{ext}, D_m, γ is not needed, the dimensionless version of the POR model can be used more easily. Then, only one parameter, St′, has to be estimated. Similarly, the application of the dimensionless version of the GR model requires only

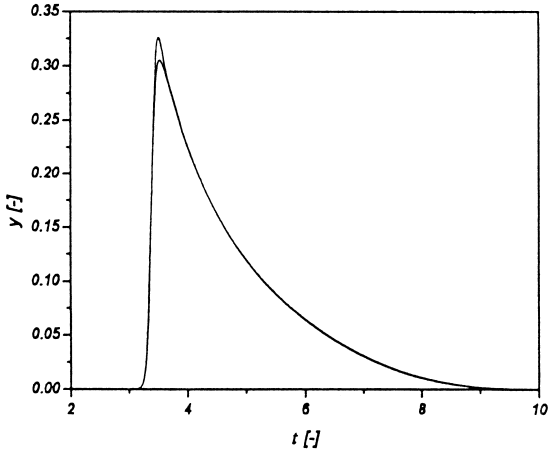

Fig. 13. Same as Fig. 12 but Pe = 4000, St′ = 100. The upper line is the solution of the POR model, the lower line that of the TD model.

two parameters instead of one for the TD model, the Stanton and the Biot numbers.

6. Nomenclature

a	Slope of a linear isotherm
a_1, a_2	First parameters of Langmuir isotherms
a_p	External surface area of the adsorbent particles
b_1	Second parameter of a Langmuir isotherm
Bi	$(k_{ext}R_p)/D_{eff}$ = Biot number
C	Concentration in the mobile phase
C_p, $\overline{C}_{p,i}$	Concentration or average concentration in the stagnant fluid phase contained in the pores
d_p	Equivalent particle diameter
D_L	Dispersion coefficient
D_m	Molecular diffusion coefficient
D_{eff}	Effective diffusion coefficient
H	Height equivalent to theoretical plates
k	Overall mass transfer coefficient
k_a	Adsorption rate constant
k_f	Overall mass transfer coefficient in TD model
k_{ext}	External mass transfer coefficient
k_{int}	Internal mass transfer coefficient
k'_0	Retention factor
k_1	Analog to the retention factor, see Eq. (34)
L	Column length
Pe	$(uL)/(D_L\epsilon_e)$ = Peclet number
q, $\overline{q}$	Concentration in the solid phase
Q, $\overline{Q}$	Dimensionless or average dimensionless concentration in the solid phase
r	Radial coordinate
R	Dimensionless radial coordinate
R_p	Equivalent particle radius
Re	$(\rho u_f d_p)/\eta$ = Reynolds number
Sc	$\eta/(\rho D_m)$ = Schmidt number
Sh	$(k_{ext}d_p)/D_m$ = Sherwood number
St	$(k_{ext}a_pL\epsilon_e)/u$; $St'_i = [St_i/(1+Bi/5)] = (k_i a_p L\epsilon_e)/u$; $St''_i = (k_{f,i}L\epsilon_e)/u$ = Stanton numbers
t	Time
t_p	Time during the constant concentration is fed into column
u	Superficial velocity
x	Dimensionless axial coordinate
y	Dimensionless concentration in moving fluid phase
y, $\overline{y}_p$	Dimensionless concentration or average dimensionless concentration in the stagnant fluid phase in the pores
z	Axial coordinate

Greeks

γ	Tortuosity parameter
ϵ_e, ϵ_p, ϵ_T	External, internal and total porosities
η	Viscosity of fluid phase
ρ	Fluid molar density
τ	Dimensionless time
τ_p	Dimensionless time during the constant concentration is fed into column

Subscripts

i	Component index
r	Reference conditions
s	Solid phase
f	Inlet value

Superscripts

0	Initial value
*	Equilibrium value

Acknowledgements

This work was supported in part by grant CHE-0070548 from the National Science Foundation and by the cooperative agreement between the University of Tennessee and the Oak Ridge National Laboratory.

References

[1] D.M. Ruthven, Principles of Adsorption and Adsorption Processes, Wiley, New York, 1984.
[2] M. Suzuki, Adsorption Engineering, Elsevier, Amsterdam, 1990.
[3] G. Guiochon, S.G. Shirazi, A.M. Katti, Fundamentals of Preparative and Nonlinear Chromatography, Academic Press, Boston, MA, 1994.
[4] K. Kaczmarski, G. Storti, M. Mazzotti, M. Morbidelli, Comput. Chem. Eng. 21 (1997) 641.

[5] A.J. Berninger, R.D. Whitley, X. Zhang, N.-H.L. Wang, Comput. Chem. Eng. 15 (1991) 749.
[6] P. Sajonz, H. Guan-Sajonz, G. Zhong, G. Guiochon, Biotechnol. Prog. 12 (1997) 170.
[7] K. Miyabe, G. Guiochon, Biotechnol. Prog. 15 (1999) 740.
[8] K. Miyabe, G. Guiochon, J. Chromatogr. A 866 (2000) 147.
[9] M. Friedrich, A. Seidel, D. Gelbin, Chem. Eng. Process 24 (1988) 33.
[10] K. Lederer, I. Amtmann, S. Vijaykumar, J. Billiani, J. Liq. Chromatogr. 13 (1990) 1849.
[11] D. Leaist, L. Hao, J. Chem. Soc., Faraday Trans. 89 (1993) 2775.
[12] S. Gibbs, A. Chu, E.N. Lightfoot, T. Root, J. Phys. Chem. 95 (1991) 467.
[13] B. Al-Duri, G. McKay, J. Chem. Technol. Biotechnol. 55 (1992) 245.
[14] W. Gallagher, C. Woodward, Biopolymers 28 (1989) 2001.
[15] A. Seidel-Morgernstern, S.C. Jacobson, G. Guiochon, J. Chromatogr. 637 (1993) 19.
[16] K. Kaczmarski, D. Antos, J. Chromatogr. A 756 (1996) 73.
[17] H. Guan-Sajonz, P. Sajonz, G. Zhong, G. Guiochon, Biotechnol. Prog. 12 (1996) 380.
[18] T. Gu, G.J. Tsai, G.T. Tsao, in: A. Fiechter (Ed.), Advances in Biochemical Engineering/Biotechnology 49, Springer-Verlag, Berlin Heidelberg, 1993.
[19] K. Kaczmarski, Comput. Chem. Eng. 20 (1996) 42.
[20] M. Morbidelli, A. Servida, G. Storti, S. Carra, Ind. Eng. Chem. (Fundam.) 21 (1982) 123.
[21] M. Morbidelli, G. Storti, S. Carra, G. Niederjaufner, A. Pontoglio, Chem. Eng. Sci. 39 (1984) 383.
[22] J. Jacobson, J.H. Frenz, Cs. Horvath, Ind. Eng. Chem. (Res.) 26 (1987) 43.
[23] E.J. Wilson, C.J. Geankoplis, Ind. Eng. Chem. (Fundam.) 5 (1966) 9.
[24] P. Rouchon, M. Schonauer, P. Valentin, G. Guiochon, Sep. Sci. Technol. 22 (1987) 1793.
[25] K. Kaczmarski, Comput. Chem. Eng. 20 (1996) 42.
[26] H.S. Tsou, E.E. Graham, AIChE J. 31 (1985) 1959.
[27] E.E. Graham, C.F. Fook, AIChE J. 28 (1982) 245.
[28] G.L. Skidmore, B.J. Horstmann, H.A. Chase, J. Chromatogr. 498 (1990) 113.
[29] M.A. Fernandez, G. Carta, J. Chromatogr. A 746 (1996) 169.
[30] M.A. Fernandez, W.S. Laughinghouse, G. Carta, J. Chromatogr. A 746 (1996) 185.
[31] H. Yoshida, M. Yoshikawa, T. Kataoka, AIChE J. 40 (1944) 2034.
[32] J.J. van Deemter, F.J. Zuiderweg, A. Klinkenberg, Chem. Eng. Sci. 5 (1956) 271.
[33] L. Lapidus, N.R. Amundson, J. Phys. Chem. 56 (1952) 984.
[34] E. Kucera, J. Chromatogr. 19 (1965) 237.